Emissivity of rough sea surface for 8–13 μm: modeling and verification

Xiangqian Wu and William L. Smith

The emissivity model for rough sea surface [Remote Sensing Environ. **24,** 313–329 (1988)] is inspected in light of the measured surface emissivity. In the presence of moderate wind (5 m/s or less), the emissivity model is found to be adequate for small to moderate view angles. For large view angles, the discrepancy between the computed and the measured emissivity is large, but one can reduce this considerably by incorporating the reflected sea surface emission into the emissivity model. In addition, examination of the spectral variation of the observed and computed emissivity suggests the need for refined measurements of the complex refractive index. An improved model is constructed to calculate the rough sea surface emissivity that can be used to provide accurate estimates of sea surface skin temperatures from remotely sensed radiometric measurements. An important feature of the improved model is that the computed sea surface emissivity is only weakly dependent on wind speed for most view angles used in practice.

Key words: Emissivity of rough sea surface, sea surface temperature, infrared remote sensing.

1. Introduction

The emissivity of the world's ocean surface in the atmospheric window spectrum (8–13 μm) is an important parameter for retrieving the sea surface temperature (SST) from remotely sensed radiometric measurements, such as from satellites. It has been established that the SST must be estimated to within 0.3 K for climate research.[1] Consequently, the sea surface emissivity needs to be determined with an accuracy of 0.5%.[2] This accuracy has not been achieved. In most SST retrieval algorithms, the sea surface emissivity has been assumed, explicitly or implicitly, to be either unity or a constant (e.g., 0.98). This assumption, largely because of the lack of knowledge about the sea surface emissivity, is often in error by more than 1% (see Fig. 3).

The physics of modeling the water surface emissivity has been known since the last century, but the computational requirement made the modeling intractable before the proliferation of electronic computers. Hall[3] computed the emissivity of specular water surface and speculated that the decrease of the measured brightness temperature with increasing view angle may be caused largely by the emissivity variation, rather than the atmospheric absorption. To explore the shadowing effects of the rough sea and its link to the existence of the oceanic horizon, Saunders[4] used the slope distribution statistics compiled by Cox and Munk[5] to compute the rough sea surface reflectivity, a quantity closely related to the rough sea surface emissivity. The scheme outlined by Saunders was used, apparently independently, by Takashima and Takayama,[6] who numerically evaluated the rough sea surface emissivity. This research was improved subsequently by Masuda *et al.*,[7] who took into account the effect of salinity on the refractive index and the shadowing effect of waves, used the complex form of Snell's law and Fresnel's formula, and corrected a typographic error for the refractive index at 10 μm. The emissivity model by Masuda *et al.* has been well received and referenced by more than 30 papers since its publication. Using satellite data, radiosonde, and a radiative transfer model, François and Ottlé[8] found that the ratio of sea surface emissivity around the nadir to those between 52°–55° generally agree with the results by Masuda *et al.* Except for this, verification of the emissivity model by laboratory or field experiments, or confirmation by other theoretical studies, has not been available.

Our purpose in this paper is to verify and improve the emissivity modeling by the measurements of

The authors are with the Cooperative Institute for Meteorological Satellite Studies, Space Science and Engineering Center, University of Wisconsin, 1225 West Dayton Street, Madison, Wisconsin 53706.

Received 2 January 1996; revised manuscript received 16 September 1996.

0003-6935/97/122609-11$10.00/0

the rough sea surface emissivity for 8–13 μm, made available recently during a field experiment.[9] After critically reviewing Masuda's emissivity model and summarizing the major characteristics of the measured sea surface emissivity, we compare the computed emissivity with the measurements. The discrepancy between the computed and observed emissivity reveals the importance of a mechanism called reflected emission. The spectral variations of the observed and computed emissivity are also examined, suggesting the need for refined laboratory data of the refractive index for sea water. Finally, the significance of the improved sea surface emissivity model relevant to SST retrieval is discussed.

We make a distinction concerning the definitions. Unless otherwise specified, emissivity, reflectivity, transmittance, and absorptance are used here for radiance. They differ from their counterparts for irradiance, as commonly defined in textbooks, in that the latter involve the integration over solid angles.

2. Computation of Rough Sea Surface Emissivity

A. Physical Basis

At the air–sea interface, Fresnel's formula[10] states that the amplitude of the reflected electromagnetic waves relative to the incident waves in the two polarizations $\rho_\parallel$ and $\rho_\perp$ are given by

$$\rho_\parallel = \frac{n\cos\chi - \cos\chi'}{n\cos\chi + \cos\chi'}, \tag{1}$$

$$\rho_\perp = \frac{\cos\chi - n\cos\chi'}{\cos\chi + n\cos\chi'}, \tag{2}$$

where n is the refractive index of seawater, χ is the angle of incidence, and χ' is the angle of refraction that can be found by Snell's law:

$$\sin\chi' = (\sin\chi/n). \tag{3}$$

Because n is normally a complex number, so are χ', $\rho_\parallel$, and $\rho_\perp$. Note that Eq. (1) differs from Eq. (3) of Masuda *et al.*[7] by a negative sign. As far as the reflected energy in two polarizations is concerned, which are the squares of $\rho_\parallel$ and $\rho_\perp$, respectively, this difference does not matter. For the rigorousness of physics, we note that this difference arises from the choice of the positive direction for the parallel components of the electric vectors. As pointed out by Clarke and Grainger,[11] this is perfectly acceptable as long as the equation and the choice of a parallel component are consistent.

The total reflectivity ρ is a combination of the reflected energy in two polarizations, modulated by the sensor's sensitivity to the two polarization components. Because most sensors in use in the infrared spectrum are unpolarized (having no preference to either polarizations), the total reflectivity is defined as a simple average:

$$\rho(n, \chi) = \frac{|\rho_\parallel|^2 + |\rho_\perp|^2}{2}. \tag{4}$$

Note that the underlight (radiation scattered from particulate in the ocean back to the sensor) can be ignored here for two reasons. First, the reflectivity defined in Eq. (4) is part of the physical properties of the sea surface rather than a model for some measurements. Second, the underlight is negligible for the wavelength under consideration.[12] Now, by the conservation of energy, the photons not reflected will be transmitted through the interface and eventually absorbed by the seawater, so the absorptance of sea surface α is

$$\alpha(n, \chi) = 1 - \rho(n, \chi). \tag{5}$$

Finally, according to Kirchhoff's law for radiance (see Appendix A), the emissivity of sea surface ε is

$$\varepsilon(n, \chi) = \alpha(n, \chi) = 1 - \rho(n, \chi). \tag{6}$$

B. Application to the Real Sea Surface

Equation (6) indicates that the sea surface emissivity ε depends only on the refractive index of seawater n and the incident angle χ. To know the value of these two parameters, however, is not trivial without laboratory control. The refractive index of seawater n depends on many factors. In this paper the n is fixed for temperature, salinity, and cholorinity, but it varies with wavelength. Masuda *et al.*[7] used the refractive index compiled by Hale and Querry[13] for pure water, with adjustments by Friedman[14] for artificial ocean water for temperature at 25 °C. These values are used here initially, but later the use of the refractive indices derived by other investigators under similar conditions are discussed.

The incident angle is equal to the view angle if the reflection is specular (the sea surface is calm). When the sea surface is roughened, a sensor above the sea surface effectively receives emission from numerous small facets of the sea surface. Each facet emits at a distinct angle to the sensor. Thus the task becomes to find a mean emissivity $\bar{\varepsilon}$ that represents the integral effects of all facets. Note that $\bar{\varepsilon}$ is still a radiance emissivity; the integration refers to the contributions of individual facet to a predefined direction. In this paper, we focus attention on the sea surface roughened by wind. According to Cox and Munk,[5] the facet slope distribution of wind-roughened sea surface is approximately normal and isotropic with the probability density function

$$P(z_x, z_y) = \frac{1}{2\pi\sigma^2}\exp\left(-\frac{z_x^2 + z_y^2}{2\sigma^2}\right), \tag{7}$$

where z_x and z_y are the slopes originally along the upwind and crosswind directions. Because of the isotropy assumption, z_x and z_y are now any orthogonal slope components at the sea surface, both having zero mean and root mean square of σ. The mean-

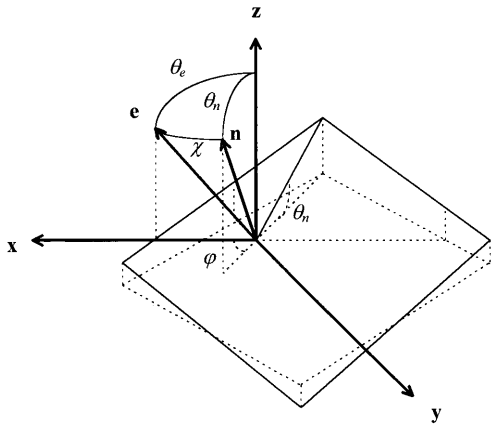

Fig. 1. Geometry of emission at a wave facet tangent to the instantaneous sea surface, after Masuda *et al.*[7] with minor modification. **z** is the local zenith; the other two orthogonal components of the Cartesian coordinate, **x** and **y**, are defined such that **e**, the unit vector of emission, is in the **x–z** plane. **n** is the facet unit normal vector; θ_n and φ are its zenith and azimuth angles, respectively. θ_e and χ are zenith angles of emission **e** relative to the local zenith **z** and the facet norm **n**, respectively.

square slope σ^2 is found to increase nearly linearly with w, the wind speed (in meters per second), at masthead [41 ft (12.5 m) above the sea surface] to w = 14 m/s:

$$2\sigma^2 = 0.003 + 0.00512w. \tag{8}$$

In addition to the ocean waves, other natural processes can affect the sea surface emissivity. The sea surface is sometimes coated with a film of oil of biological or petrochemical origin; the latter can be caused by either natural seepage or human activity. The oil slicks tend to reduce the surface tension, hence suppress capillary waves and reduce the sea surface roughness under similar wind conditions.[5] Meanwhile, the refractive index at the sea surface will change in accordance with the composition and the thickness of the oil slicks.[15] The sea surface can also be covered partially by the whitecaps that start to appear with increasing wind speed (>10 m/s) as a result of the wave breaking at the crest.[16] The whitecaps consist of a thin layer of foam or small bubbles at the sea surface. They certainly have an effect on the reflectance in the visible region of the spectrum, as the name whitecaps suggests. Their impact on the infrared emissivity, however, is unclear. Nevertheless, the oil slicks and whitecaps are not modeled here because their presence, and the detailed physical processes by which they affect sea surface emissivity, are not known well enough to be included in the construction and application of the sea surface emissivity model.

The computation of the mean sea surface emissivity for a certain wavelength of radiation toward a specific direction in space can be assisted by the examination of the emission geometry at an ocean wave facet, as illustrated in Fig. 1. Before we proceed further, we recognized that, in Fig. 1, the radiation at a point on a wave facet has been approximated by a plane tangent to the facet at the point. This approximation is valid only if

$$2\pi R \cos^3 \chi \gg \lambda, \tag{9}$$

where R is the radius of facet curvature at the point, χ has been defined in Fig. 1, and λ is the wavelength in use.[17] In essence, Eq. (9) requires that the ocean wave is sufficiently smooth relative to the optical wavelength in use. For the infrared spectrum, λ is on the order of 10^{-5} m, which means that the tangent plane assumption is valid even for capillary waves. This simplification is not valid for the microwave spectrum.[18]

The slope components z_x and z_y in Fig. 1 can be expressed in terms of θ_n and φ as

$$z_x = \partial z/\partial x = -\tan\theta_n \cos\varphi, \tag{10}$$

$$z_y = \partial z/\partial y = -\tan\theta_n \sin\varphi. \tag{11}$$

By the cosine theorem of spherical trigonometry, the zenith angle χ of emission **e** relative to the facet norm **n** is

$$\begin{aligned}\cos\chi &= \cos\theta_e \cos\theta_n + \sin\theta_e \sin\theta_n \cos\varphi \\ &= \mu_e\mu_n + (1-\mu_e^2)^{1/2}(1-\mu_n^2)^{1/2}\cos\varphi,\end{aligned} \tag{12}$$

where $\mu_e = \cos\theta_e$ and $\mu_n = \cos\theta_n$.

According to the slope distribution probability density function [Eq. (7)], the probability for slope of $(z_x \pm dz_x/2, z_y \pm dz_y/2)$, or the fractional horizontal area with that slope, is $P(z_x, z_y)dz_xdz_y$. Projected to the facet surface, the fractional area becomes $\mu_n^{-1}P(z_x, z_y)dz_xdz_y$. If R is the blackbody radiance at the sea surface for the wavelength in question, the radiance from a unit area on the facet to **e** is $\varepsilon(n, \chi)R\cos\chi$, and the contribution from this facet to radiance along **e** is $\varepsilon(n, \chi)R\cos\chi\mu_n^{-1}P(z_x, z_y)dz_xdz_y$. We can then obtain the total radiance along **e** by adding up such contributions from all possible facets. On the other hand, if the mean emissivity along **e** is $\bar{\varepsilon}'(n, \mu_e)$, the total radiance along **e** is simply $\bar{\varepsilon}'(n, \mu_e)R\mu_e$, thus:

$$\begin{aligned}\bar{\varepsilon}'(n, \mu_e) = \frac{1}{\mu_e}\int_{-\infty}^{\infty}\int_{-\infty}^{\infty} &\varepsilon(n, \chi)\cos\chi\mu_n^{-1} \\ &\times P(z_x, z_y)dz_xdz_y, \qquad \cos\chi > 0.\end{aligned} \tag{13}$$

Considering Eqs. (10) and (11), $P(z_x, z_y)$ can be expressed in terms of θ_n as

$$P(\theta_n) = \frac{1}{2\pi\sigma^2}\exp\left(-\frac{\tan^2\theta_n}{2\sigma^2}\right), \tag{14}$$

and the slope increments dz_xdz_y can be converted to angular increments $d\mu_nd\varphi$ as

$$dz_xdz_y = |J|d\mu_nd\varphi = \mu_n^{-3}d\mu_nd\varphi, \tag{15}$$

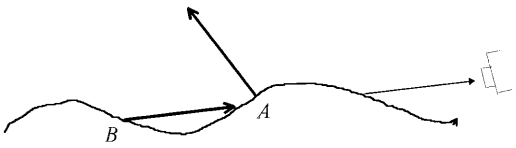

Fig. 2. Illustration of the wave shadowing of emission.

where J is the Jacobian:

$$J = \begin{vmatrix} \frac{\partial z_x}{\partial \mu_n} & \frac{\partial z_x}{\partial \varphi_n} \\ \frac{\partial z_y}{\partial \mu_n} & \frac{\partial z_y}{\partial \varphi_n} \end{vmatrix}. \tag{16}$$

Finally, substituting Eqs. (14) and (15) into Eq. (13) and noting that cos χ [Eq. (12)] is an even function with respect to φ_n [thus so is $\varepsilon(n, \chi)$, Eqs. (1)–(6)], we obtain

$$\bar{\varepsilon}'(n, \mu_e) = \frac{1}{\pi\sigma^2\mu_e}\int_0^1\int_0^\pi \varepsilon(n, \chi)\cos\chi \exp\left(\frac{-\tan^2\theta_n}{2\sigma^2}\right) \times {\mu_n}^{-4} d\varphi d\mu_n, \quad \cos\chi > 0. \tag{17}$$

C. Wave Shadowing

As μ_e approaches zero (viewed at grazing angle), one expects the mean emissivity to diminish. Instead, the mean emissivity computed by Eq. (17) becomes unbounded. This is because of the omission of the wave shadowing. As depicted in Fig. 2, emission from the sea surface can be blocked by waves in two ways. At point A, radiation propagates away from the direction of the sensor. This self-blocking by waves can be excluded by imposing cos $\chi > 0$ in Eq. (17). At point B, however, emission that would reach the sensor is blocked by other waves. This interblocking by waves has not been treated properly in Eq. (17).

For this paper, we devised a scheme to correct the interwave blocking using a heuristic approach. Except for the grazing angle, if the emissivity toward any other direction is identically unity, $\varepsilon(n, \chi) \equiv 1$, the mean emissivity to those directions must also be unity, $\bar{\varepsilon}'(n, \mu_e) \equiv 1$. But if $\varepsilon(n, \chi) \equiv 1$ is used in Eq. (17), one finds, typically, that

$$\Sigma(\mu_e) = \frac{1}{\pi\sigma^2\mu_e}\int_0^1\int_0^\pi \cos\chi \exp\left(\frac{-\tan^2\theta_n}{2\sigma^2}\right) \times {\mu_n}^{-4} d\varphi d\mu_n, \qquad \cos\chi > 0 \tag{18}$$

remains unity only for $\theta_e < 80°$ at light wind (1 m/s) or $\theta_e < 60°$ for strong wind (15 m/s). For a larger view angle or wind speed, or both, $\Sigma(\mu_e) > 1$. This is not attributable to the numerical scheme used (see Table 1 and the discussion in Subsection 2.D), rather it is a manifestation of the wave shadowing as illustrated in Fig. 2: $\Sigma(\mu_e) > 1$ because the hidden areas have been included incorrectly in the integration. An effective way to eliminate this shadowing effect, therefore, is to define the mean emissivity as $\bar{\varepsilon}'$ normalized by $\Sigma(\mu_e)$:

$$\bar{\varepsilon}(n, \mu_e) = \frac{\bar{\varepsilon}'(n, \mu_e)}{\Sigma(\mu_e)}. \tag{19}$$

An assumption implied in this scheme is that the slope distribution of the hidden areas is the same as that for the whole population. This is true for the normally distributed wave slopes defined in Eq. (7).

Several authors have investigated the problem of wave shadowing. Using a similar argument in the study of shadowing effects of waves on reflection at the sea surface, Saunders[4] arrived at the same solution; Eq. (9) of Saunders is equivalent to Eq. (18) here. Furthermore, Saunders noticed that the results from these equations compared favorably with a much more detailed theoretical study by Wagner,[19] with results from a numerical simulation study by Brockelman and Hagfors,[20] and with the actual measurements by Hamilton.[21] Recently, Yoshimori *et al.* used a similar approach with more rigorous analysis and supporting observations to study the shadowing effect in one-dimensional[22] and two-dimensional[23] cases.

Masuda *et al.*[7] realized that one of the flaws in the computation of the rough sea surface emissivity by Takashima and Takayama[6] was the unboundedness of $\bar{\varepsilon}(n, \mu_e)$ toward the grazing angle. They suspected that this defect was related to the wave shadowing, and they derived a correction scheme, identical to Eq. (19), from an energy conservation point of view. However, they were uncertain as to whether the normalization procedure is indeed necessitated by the wave shadowing and, conversely, if Eq. (19) is sufficient to account for the shadowing effect. Later they realized the equivalence of their Eq. (20) and Saunders's Eq. (10).[24]

D. Numerical Scheme

A recursive Simpson quadrature algorithm[25] was used for the double integration of Eqs. (17) and (18). The algorithm uses Simpson's rule and progressively refines the quadrature interval until a prescribed accuracy is achieved. This numerical technique is accurate because it uniformly guarantees the required accuracy throughout the integration, which is especially important for double integration. It is also economic because it requires only $N + 1$ function evaluations for quadrature with N intervals, where N is self-adjusted to meet the required accuracy.

As θ_n approaches 90°, the integration over azimuth angle φ remains finite, but $\exp(-\tan^2\theta_n/2\sigma^2){\mu_n}^{-4}$ vanishes. This suggests that the numerical efficiency can be improved by raising the lower bound of the outer integration in Eqs. (17) and (18) from 0 to ${\mu_n}^*$, where ${\mu_n}^*$ satisfies

$$\exp\left(\frac{{\mu_n}^{*2} - 1}{2\sigma^2{\mu_n}^{*2}}\right) < \delta{\mu_n}^{*4} \le \delta,$$

Table 1. Integration of Eq. (18) with Various δ for $\theta_e = 73.5°$ and $w = 16$ m/s

δ	$\Sigma(\mu_e)$
10^{-2}	1.00664
10^{-3}	1.02196
10^{-4}	1.02333
10^{-5}	1.02346
10^{-6}	1.02347
10^{-7}	1.02347

which is equivalent to

$$\mu_n^* > (1 - 2\sigma^2 \ln \delta)^{-1/2}, \tag{20}$$

where δ is the required accuracy. This may reduce the integration interval considerably. For example, for wind speeds of 0, 1, 3, 5, 10, and 15 m/s, using Eq. (8) and assuming $\delta = 10^{-5}$, we found μ_n^* to be 0.9832, 0.9563, 0.9077, 0.8673, 0.7932, and 0.7219, respectively.

The above scheme has been applied to the integration of Eq. (18) with various convergence criteria δ. Table 1 presents the results for a view angle of 73.5° and a wind speed of 16 m/s; results for other view angles and wind speeds are similar. The table shows that the accuracy of $\Sigma(\mu_e)$ is an order of magnitude lower than δ. This is because the accuracy of the inner integration over azimuth angle φ is only δ, which may accumulate in the outer integration over zenith angle μ_n. The main point of Table 1, however, is that the overall accuracy of the double integration can be controlled adequately through δ, as required for any successful numerical schemes. Table 1 also eliminates the possibility that the nonunity of $\Sigma(\mu_e)$ in Eq. (18) is due to a numerical scheme. The fact that $\Sigma(\mu_e)$ remains nonunity for decreasing δ indicates that the nonunity reflects a physical reality, such as wave shadowing.

3. Observation of Rough Sea Surface Emissivity

The ocean surface temperature and emissivity was observed on 16 January 1995 in the Gulf of Mexico (26 °N, 94 °W) with a Fourier transform spectrometer. A cold front passed the area a day earlier, with surface wind of 15 m/s. On the day of measurement, however, the sky was clear and the wind calmed down to approximately 5 m/s for the entire day. The ocean temperature was approximately 22 °C. The instrument was mounted aboard the side of an oceanographic research vessel, the *R. V. Pelican*, operated by the Louisiana University Marine Consortium. Spectral radiance from 500 to 3500 cm^{-1} (3.0 to 20 μm) was measured, with a spectral resolution of 0.5 cm^{-1}, at several view angles (36.5°, 56.5°, and 73.5°, as measured from nadir). Because these radiance measurements contain both the sea radiation emitted by the sea surface and the sky radiation reflected by the sea surface, the sky radiation was also measured quasi concurrently with the same instrument to help isolate the sea radiation.

A technique has been developed to solve the radiative transfer equation for the surface temperature and emissivity from the measurements of ocean and sky radiation. The accuracy of the determinations of temperature and emissivity are believed to be better than 0.1 °C and 0.1%, respectively, on the basis of comparisons with *in situ* ocean temperature measurements at the sea surface (at approximately 3-cm depth) and at the ship's engine intake (at approximately 2-m depth). A complete description of the spectral radiance measurements and the technique used for deriving the spectral distribution of ocean emissivity is provided by Smith *et al.*[9]

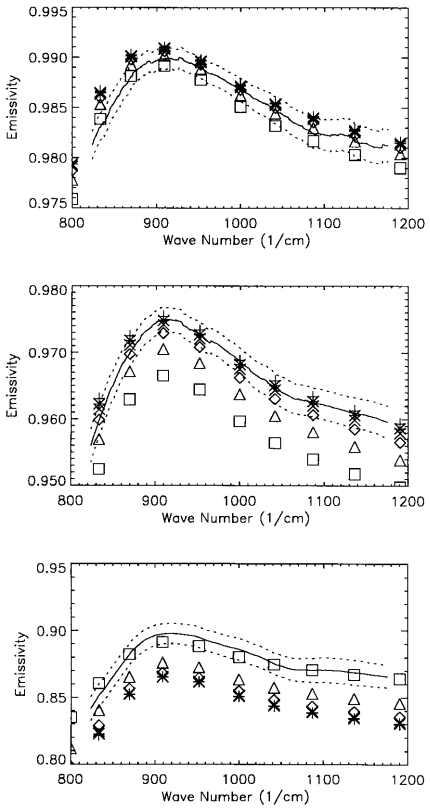

Fig. 3. Comparison of the computed and measured emissivity at 36.5° (upper), 56.5° (middle), and 73.5° (lower). Solid and dotted curves are the mean and standard deviation of the measured emissivity. Symbols mark the computed emissivity with Eq. (19) for wind speed of 0 (+), 1 (*), 2 (×), 4 (◇), 8 (△), and 16 (□) m/s.

4. Characteristics of Rough Sea Surface Emissivity

The sea surface emissivity computed by Eq. (19) agrees with those reported by Masuda *et al.*[7] to the fourth digit (the convergence criterion $\delta = 10^{-5}$ was used). This is expected, as a similar procedure and an identical refractive index are used. The computed sea surface emissivity for several view angles and wind speeds is plotted in Fig. 3. The emissivity is found to decrease with view angle, a well-known consequence of Eqs. (1)–(6). The emissivity is also found to decrease with wind speed at small angles but increases with wind speed at large angles; the reason is illustrated in Fig. 4. For a perfectly calm sea viewed from a small zenith angle (upper left panel),

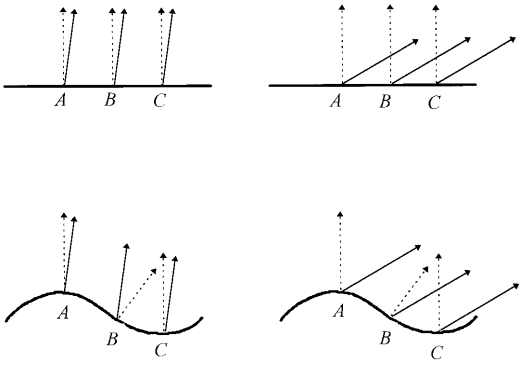

Fig. 4. Illustration of the effect of sea surface roughness on mean emissivity for small and large view angles. Solid arrowhead lines are the direction of emission and dashed arrowhead lines are the local zenith. For a small view angle (left), emission from any point (A, B, or C) has a small emission angle when the sea is calm (upper). When the sea is rough (lower), emission from crest (A) and valley (C) remains at a small emission angle, but emission from wave slope (B) has a larger emission angle. The mean emissivity thus will reduce as the sea surface becomes rough. Similarly, the mean emissivity of the sea surface will increase with surface roughness for the large view angle (right).

every point (A, B, and C) on the sea surface is viewed at a small angle and, therefore, exhibits large emissivity. When a rough sea surface is viewed at the same angle (lower left panel), the emissivity at the wave crest (point A) and valley (point C) remains large, but the emission from the wave slopes (point B) is that to a larger local zenith, thus smaller emissivity. When averaged, mean emissivity for a rough sea surface will be smaller than that for a calm sea. If the sea surface is viewed at a sufficiently large angle, on the other hand, the right column of Fig. 4 shows that the opposite may be true. The emission from a calm sea to an obliquely viewing sensor (upper right panel) are those to a large local zenith, thus smaller emissivity. The wave slopes (lower right panel) provide the opportunity for the sensor to view some parts of the water surface at a smaller local zenith (point B). The mean emissivity for a rough sea, therefore, may be larger than that for a calm sea.

In addition to its dependence on wind speed, the computed emissivity in Fig. 3 is also a function of the view angle and the wavelength. The angular dependence can be appreciated by the following example. For a wave number of 910 cm^{-1} (11 μm) and under a calm wind condition, the computed emissivity decreases by approximately 0.015, from 36.5° to 56.5°, and by approximately 0.075, from 56.5° to 73.5°. If an error of 0.01 in emissivity is equivalent to an error of 0.5 K in brightness temperature,[2] these differences in emissivity translate into a brightness temperature difference of 0.8 K and 3.8 K, respectively, which is significant when one considers the normal climatological variability of the sea surface temperature.

For the same calm wind condition, the difference between the computed emissivity at 820 and 910 cm^{-1} is approximately 0.01, 0.02, and 0.05, corresponding to a brightness temperature difference of 0.5 K, 1.0 K, and 2.5 K, for view angles of 36.5°, 56.5°, and 73.5°, respectively. A common practice among the users of the advanced very-high resolution radiometer data is to regard the brightness temperature difference between channel 4 (880–970 cm^{-1}) and channel 5 (800–880 cm^{-1}) as evidence of atmospheric water vapor absorption. It is now clear that a fairly large part of this difference may be due to the spectral variation of emissivity; the larger the view angle, the larger the part of brightness temperature difference that is caused by emissivity.

5. Improvements of the Emissivity Model

A. Reflected Emission

Also plotted in Fig. 3 as solid curves are the measured sea surface emissivity during the field experiment. These experimental results provide, for the first time as far as we know, a direct validation of the theoretical computation by Masuda *et al.*[7] The agreement is impressive, particularly for small view angles, considering that the results are from totally different approaches and are completely independent of each other. At a large view angle (73.5°), the computed emissivity is still able to capture the general spectral variation of the measured emissivity, however with a relatively constant negative bias. This suggests that the performance of the sea surface emissivity model by Masuda *et al.*[7] appears adequate in general, but it may have omitted some physical processes that become prominent at large view angles.

One candidate for such a process is the reflection of the emission from the sea surface, as illustrated in Fig. 5, that effectively enhances the sea surface emissivity. More precisely, the emissivity at point O does not change. However, because of the contribution from $\mathbf{r}$ that is reflected at O, radiance along $\mathbf{e}$ is enhanced. Because the blackbody radiance at any point of the sea surface to any direction is a constant R, the enhancement of radiance is equivalent to an enhancement of emissivity. In other words, the effective emissivity $\tilde{\varepsilon}(n, \chi)$ can be defined as

$$\tilde{\varepsilon}(n, \chi) = \varepsilon(n, \chi) + [1 - \varepsilon(n, \chi)]P(\theta_r)\bar{\varepsilon}(n, \mu_r), \quad (21)$$

where $\varepsilon(n, \chi)$ is the emissivity at point O that can be obtained from Eq. (6). $P(\theta_r)$ is the probability that radiance arriving at point O with local zenith θ_r originates from the sea surface instead of from the sky. $\bar{\varepsilon}(n, \mu_r)$, where $\mu_r = \cos \theta_r$, is the mean emissivity of the sea surface that contributes to radiance $\mathbf{r}$. $P(\theta_r)$ and μ_r are defined in detail below. The effective emissivity $\tilde{\varepsilon}(n, \chi)$ will then replace the $\varepsilon(n, \chi)$ in Eq. (17).

Otterman *et al.*[26] have speculated on the mechanism of the surface-emitted surface-reflected (SESR) radiation. They presented a mostly qualitative analysis to show that the SESR is not important for $\theta_e < 30°$. Watts *et al.*[27] further elaborated on the SESR. Their approach is similar to Eq. (21), except that in this paper we use a more sophisticated and accurate numerical scheme that, for example, can

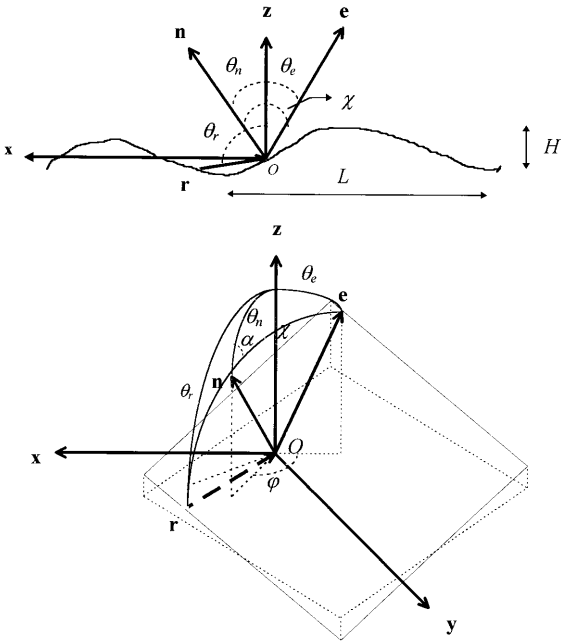

Fig. 5. Geometry of emission and reflection at a wave facet tangent to the instantaneous sea surface at point O, modified from Fig. 1. The direction of emission **e** now is such that some emission from below the horizon **r** can be reflected at point O along **e**. The two-dimensional graph (upper) illustrates this mechanism; the three-dimensional graph (lower) defines the relevant angles (see text).

distinguish the shadowing effect from digitization error.

We modeled the reflected emission $\bar{\varepsilon}(n, \mu_r)$ by considering an imaginary sensor at point O toward the opposite direction of **r**. The emissivity that the sensor measures will then be $\bar{\varepsilon}(n, \pi - \theta_r)$, assuming the sensor's field of view possesses the same statistics as that of the entire sea surface. Admittedly, this assumption seems rather doubtful at first because point O is distributed randomly on wave slopes, and the field of view of the imaginary sensor at point O is normally quite small. It is important, however, to realize that such reflection presumably will happen at a large number of points such as O. The summation of all their fields of view will be sufficiently large to resemble the population statistics.

To decide $P(\theta_r)$ in Eq. (21), note that in Fig. 5 the reflected emission is indeed from the sea surface if $\theta_r > 90°$. When θ_r is slightly less than 90°, however, it is still possible that the reflected emission is from the opposite wave slope, depending on the location of O on the slope and the steepness of the nearby slopes. If the wave height is H and the wavelength is L, then

$$\theta_r^* = \frac{\pi}{2} - \tan^{-1}\left(\frac{2H}{L}\right), \tag{22}$$

where θ_r^*, the smallest zenith angle for the sea surface emission to be reflected at O, has a theoretical lower bound of 74° from Stokes' theory and is observed to be in the range from 84° to 87° for winds to 15 m/s.[23] Because only a few reflection points near the trough can realize the full advantage of the steepness of the sea, the $P(\theta_r)$ thus should be unity for $\theta_r > 90°$, monotonically decreasing from unity to zero for θ_r ranging from 90° to θ_r^* and remain zero for $\theta_r < \theta_r^*$. Because we lacked additional knowledge, 85° was chosen for θ_r^*, and the $P(\theta_r)$ for $90° > \theta_r > \theta_r^*$ was assumed to be parabolic. In summary, the following is prescribed for $P(\theta_r)$:

$$P(\theta_r) = \begin{cases} 1, & \theta_r > 90° \\ 1 - (\theta_r - 85°)^2/25, & 85° \le \theta_r \le 90°. \\ 0, & \theta_r < 85° \end{cases} \tag{23}$$

Based on the above analysis, the reflected emission is modeled as follows. First, $\bar{\varepsilon}(n, \mu_e)$ is computed from Eq. (19) for $\theta_e \in [0,95°]$ without consideration of the reflected emission [$\bar{\varepsilon}(n, \mu_r) \equiv 0$ in Eq. (21)]. After this is computed, $\tilde{\varepsilon}(n, \chi)$ can be computed with Eq. (21) with $P(\theta_r)$ from Eq. (23) and $\bar{\varepsilon}(n, \mu_r) = \bar{\varepsilon}[n, \cos(\pi - \theta_r)]$. One could, in theory, repeat this process to simulate the multiple reflection. We found, however, that the contribution by additional reflections is negligible. For example, the reflected emission effectively increases the emissivity by 2.71% for a wavelength of 11 μm, a wind speed of 16 m/s, and a view angle of 73.5°; the additional multiple reflection adds another 0.06%.

So far it has not been shown how to compute the angle θ_r. This can again be accomplished by spherical trigonometry with the help of Fig. 5. According to the cosine theorem α, the azimuth angle between **z** and **e** relative to **n** can be computed from

$$\cos\alpha = \frac{\cos\theta_e - \cos\chi\cos\theta_n}{\sin\chi\sin\theta_n}. \tag{24}$$

The angle between **r** and **n**, according to Snell's law, is the same as that between **n** and **e**, i.e., χ. Also, according to Snell's law, the three vectors **r**, **n**, and **e** are coplanar, therefore the azimuth angle between **z** and **r** relative to **n** is $\pi - \alpha$. So the angle θ_r can be found by applying the cosine theorem:

$$\begin{aligned} \cos\theta_r &= \cos\chi\cos\theta_n + \sin\chi\sin\theta_n\cos(\pi - \alpha) \\ &= 2\cos\chi\cos\theta_n - \cos\theta_e. \end{aligned} \tag{25}$$

The effective mean emissivity, with the reflected emission modeled by Eq. (21), is plotted in Fig. 6. The observed emissivity is also plotted for comparison. It is quite convincing that the negative bias of the computed emissivity by Eq. (19) can be removed by the inclusion of the reflected emission. Nevertheless, it is perhaps premature to claim that the omission of the reflected emission is the only cause of the underestimate of the effective mean emissivity at large view angles and, presumably, at large wind speeds as well. However, the importance of the reflected emission when one computes the effective mean emissivity can be tested by an experiment. Recall that when viewed at small angles, the effect of the wave slopes is to reduce the possibility that a

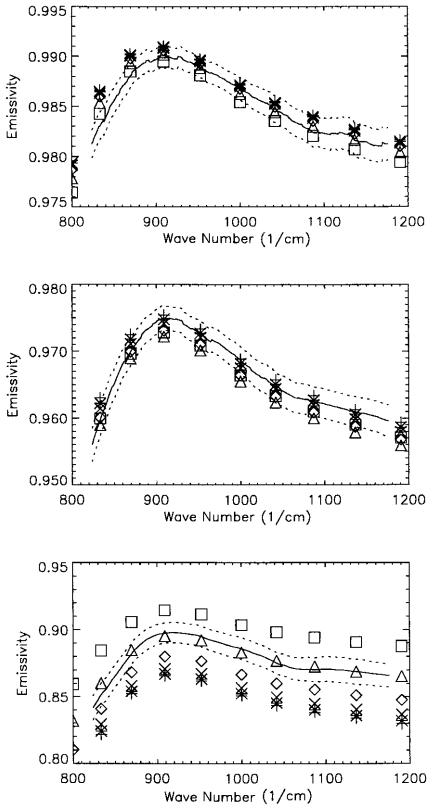

Fig. 6. As Fig. 3, but the emissivity is computed with Eq. (21) which includes the reflected emission.

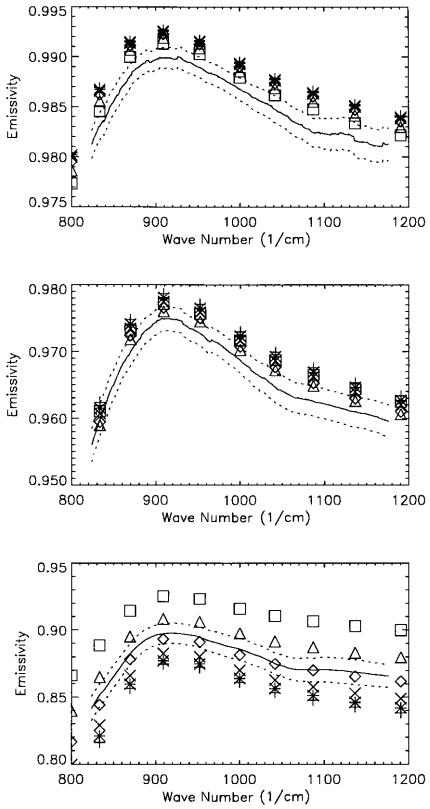

Fig. 7. As Fig. 6, but is computed with Segelstein's[29] refractive index for pure water.

facet is viewed at a smaller local zenith angle, thus reducing the mean emissivity (Fig. 4). However, these same slopes will now increase the possibility of emission reflecting from the sea surface (Fig. 5). The combined effect is a reduced sensitivity of the effective mean emissivity to the roughness of the sea surface at small to moderate view angles. This is why, compared with the results by the emissivity model without the reflected emission (Fig. 3), the model that includes the reflected emission (Fig. 6) predicts a smaller decrease of emissivity with wind speed at small and, especially, at moderate view angles. At large view angles, on the other hand, the inclusion of the reflected emission amplifies the increase of emissivity with wind speed. The hypothesis that the reflected emission is important in computing the effective mean emissivity, therefore, can be verified by measuring the sea surface emissivity at varying wind speeds, particularly around a view angle of 50°–60°.

B. Refractive Index

A close examination of Figs. 3 and 6 reveals a subtle difference in the spectral variation of the computed and measured sea surface emissivity. From 900 to 830 cm^{-1} (11–12 μm), in particular, the computed emissivity does not drop as fast as the observed emissivity. Though a small discrepancy compared with the negative bias just discussed, it warrants further investigation because this spectral region is of special importance in remote sensing of the sea surface through the atmosphere.

Unlike the negative bias, the discrepancy in the spectral variation seems to be independent of the view angle and wind speed. Accordingly, we assumed that the cause of this discrepancy is also independent of the view angle and wind speed. One possible cause is the value of the refractive index we used in computing the emissivity. The published data for the refractive index of pure water, though abundant, lack of consistency in procedure and value. For seawater, few studies quantify the salinity effects on the refractive index.

In previous computations, the value of the refractive index for pure water by Hale and Querry[13] has been used with a seawater adjustment by Friedman.[14] This is the same procedure used by Masuda *et al.*[7] Later, the refractive indices published by Pontier and Dechambenoy,[28] Segelstein,[29] and Wieliczka *et al.*[30] have been tested. It was found that the refractive index compiled by Segelstein, together with Friedman's correction for seawater, gives the best results for modeling the observed spectral variation of seawater emissivity in 11–12 μm (Fig. 7).

Unlike many other data sets that are based normally on one investigator's laboratory measurements with one type of procedure and instrument, Segelstein compiled scores of published data and strove for consistency. This may lend more credibility to the results. However, it is believed that the uncer-

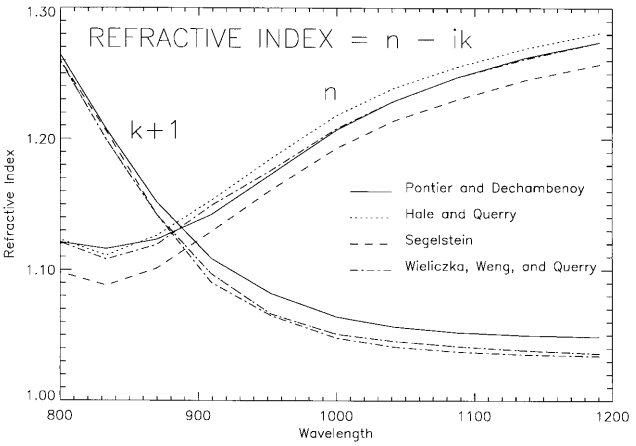

Fig. 8. Spectral variation of refractive indices obtained by various authors.

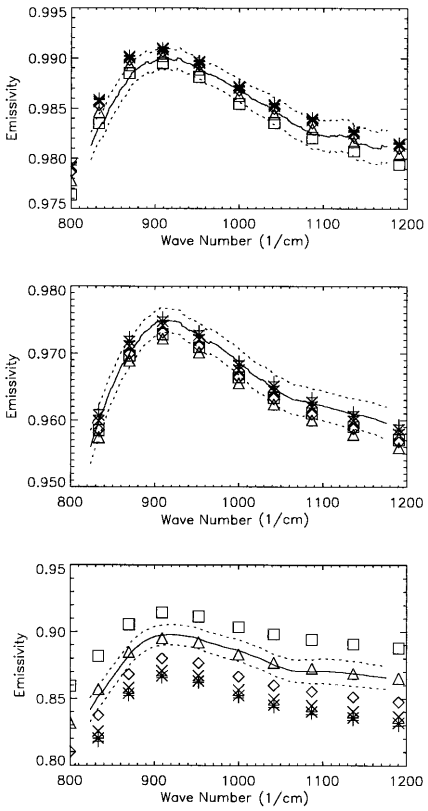

Fig. 9. As Fig. 7, but is computed with the real part of the refractive index from Hale and Querry.[13]

tainty in the refractive index for water may still cause noticeable error when emissivity is computed. For example, although Segelstein's data did the best to model the spectral variation of emissivity in the 11–12-μm region, they nevertheless seem to introduce a small amount of positive bias throughout the spectrum. This seems to be attributable to the real part of his refractive index data. Segelstein actually compiled only the imaginary part of the refractive index from the literature. Based on the Kramers–Kronig relationship, Fourier transform was then applied on the compiled data to obtain the real part of the refractive index.

It is beyond the scope of our research here to discuss the validity of the refractive index data by Segelstein or by any other investigator. We note, however, that the real part of the refractive index obtained by Segelstein seems distinctively different from those by others (Fig. 8). Using the real part of the refractive index by Hale and Querry[13] and the imaginary part by Segelstein,[29] together with the seawater adjustment by Friedman,[14] we found that the simulated emissivity matches the observations much better than using any other available refractive index (Fig. 9). This, however, does not mean that the correct refractive index for seawater has been found. Rather, it calls for more studies about the refractive index of water and, especially, about the effects of salinity and other solutes in seawater on the refractive index.

6. Summary

The sea surface emissivity needs to be known within 0.5% so as to retrieve the sea surface temperature with an accuracy of 0.3 K.[2] The sea surface temperature is not only a crucial parameter for weather and climate studies and operational forecasting, it is also a boundary condition for radiatively retrieving many other geophysical variables. In that regard, the sea surface emissivity is a cornerstone parameter required for remote sensing over the oceans.

In this paper we developed an emissivity model, with a rigorous basis in physics, for the rough sea surface and compared the model with the observation of sea surface emissivity during a field experiment. The accuracy of the observed sea surface emissivity is approximately 0.1% and has been documented in detail elsewhere.[8] These measurements of sea surface emissivity provided for the first time a direct validation of the sea surface emissivity model by Masuda *et al.*,[7] which is shown to be adequate for view angles to approximately 60°. For larger view angles, the emissivity computed by Masuda *et al.* is smaller than that observed.

It is hypothesized that the negative bias of the computed emissivity at large angles is, at least partially, caused by the omission of the sea surface emission reflected to the sensor. The inclusion of this mechanism can remove the negative bias in the simulated emissivity. An experiment was proposed to verify the importance of the reflected emission in modeling the sea surface emissivity. The final conclusion must await the measurements of emissivity for varying wind speeds.

One may wonder why the emissivity at large view angles is of concern, as most satellite instruments do not operate at those angles. The purpose is to verify the physical processes that affect the sea surface emissivity being modeled. If the simulation of the reflected emission is basically correct, the sensitivity of the sea surface emissivity to sea surface roughness can be reduced. Figure 10 shows the sensitivity of

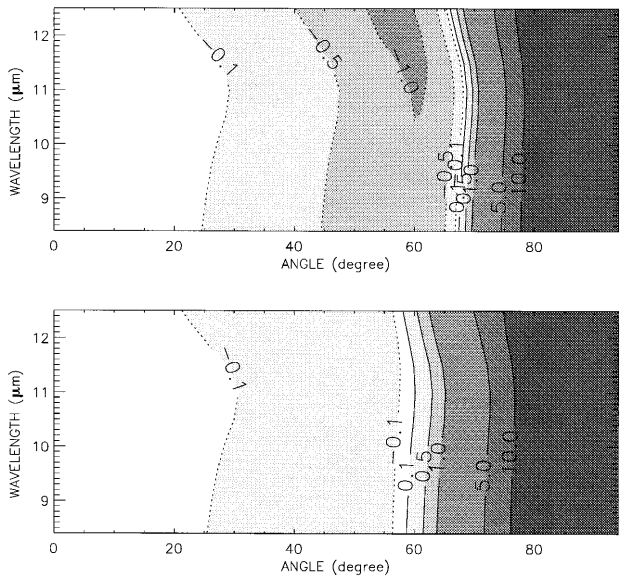

Fig. 10. Difference between the emissivity for a wind speed of 16 m/s and that for a wind speed of 0 m/s (but not the specular surface), as a function of wavelength and view angle. The model that neglects the reflected emission (upper panel) results in the difference larger than 0.5% for most angles beyond approximately 45°. The model that takes into account the reflected emission (lower panel) keeps the difference less than 0.5% for angles to approximately 60°.

the computed emissivity to wind speed. Without the reflected emission (upper panel), one needs to know the wind speed so as to model the emissivity for most view angles larger than approximately 45°; otherwise the accuracy of the modeled emissivity, especially in the 10.5–12.5-μm spectral region, may well exceed the 0.5% requirement. With the reflected emission, on the other hand (lower panel), one can assume that the emissivity is independent of the wind for view angles to approximately 60°. Because accurate estimates of the sea surface wind and roughness have been scarce in the past and remain difficult at present, removing the dependence of the sea surface emissivity on sea surface wind will greatly simplify the reconstruction of accurate sea surface temperature climatology.

Finally, we note that the uncertainty in the refractive index for seawater may cause considerable error in the calculated emissivity. This is especially true for 10.5–12.0 μm, a spectral region heavily used by the remote sensing community and a spectral region characterized by rapid spectral variation. Further clarification of this issue is crucial to specify accurately the sea surface emissivity.

Appendix A: Kirchhoff's Law for Radiance

This appendix is a logical extension of Kirchhoff's law as derived, for example, by Fleagle and Businger.[31] We first consider two parallel plates, infinite in extent, separated by empty space, perfectly insulated on the outside, and in thermodynamic equilibrium. Kirchhoff's law then states that $\varepsilon_\lambda = \alpha_\lambda$, where ε_λ and α_λ are spectral or monochromatic emissivity and absorptance, respectively, for irradiance. We define the spectral radiance emissivity $\varepsilon(\lambda, \chi)$ as the ratio of the emitted spectral radiation per unit solid angle to a direction to that from a blackbody at the same temperature. Spectral radiance absorptance $\alpha(\lambda, \chi)$ can be defined similarly.

We let wall 1 be a blackbody and the spectral radiance emissivity of wall 2 be the same as a blackbody except for a small interval at wavelength λ and to the direction χ. When the two walls reach the same temperature, the radiance from wall 1 to wall 2 is $R_{\lambda,T}^*$, the blackbody radiance for the wavelength λ and the equilibrium temperature T, regardless of direction. The radiance from wall 2 to wall 1 is also $R_{\lambda,T}^*$ in general, except for along the direction χ, which is $\varepsilon_2(\lambda, \chi)R_{\lambda,T}^* + [1 - \alpha_2(\lambda, \chi)]R_{\lambda,T}^*$. Because wall 2 is emitting at its maximum capacity in all other directions, it is required that, along the direction χ, $R_{\lambda,T}^* = \varepsilon_2(\lambda, \chi)R_{\lambda,T}^* + [1 - \alpha_2(\lambda, \chi)]R_{\lambda,T}^*$, or $\varepsilon_2(\lambda, \chi) = \alpha_2(\lambda, \chi)$. If we apply this argument to another wavelength and direction, we find that Kirchhoff's law for radiance $\varepsilon(\lambda, \chi) = \alpha(\lambda, \chi)$ is analogous to Kirchhoff's law for irradiance $\varepsilon_\lambda = \alpha_\lambda$.

Finally, we note that, although the assumptions of thermal and radiative equilibria are useful in derivation, they do not restrict the validity of Kirchhoff's law for radiance. Thermodynamic equilibrium, on the other hand, is required.

We greatly benefited from valuable discussions with K. Masuda on his past research and recent thoughts related to the issue of the sea surface emissivity. C. Velden initially introduced to us the research by Masuda *et al*. W. McKeown drew our attention to the paper by Blume *et al*. An anonymous reviewer pointed out to us the references by Yoshimori *et al*. Correspondence with P. Watts helped us understand his related research and clarified the explanation of Eq. (21). J. Phillips repeatedly surprised us with her skill and efficiency in reference searches. We are grateful for the many comments and encouragement from our colleagues at the Cooperative Institute for Meteorological Satellite Studies, particularly from B. Burns and R. Knuteson. This research was supported by NASA contract NAS5-31361.

References

1. F. Webster and M. Fieux, "TOGA overview," in *Large-scale Oceanographic Experiments and Satellites*, C. Gautier and M. Fieux, eds. (Reidel, Dordrecht, 1984), pp. 17–24.
2. X. Wu and W. L. Smith, "Sensitivity of sea surface temperature retrieval to sea surface emissivity," ACTA Meteorol. Sinica **10,** 376–384 (1996).
3. F. F. Hall, "The polarized emissivity of water in the infrared," Appl. Opt. **3,** 781–782 (1964).
4. P. M. Saunders, "Shadowing on the ocean and the existence of the horizon," J. Geophys. Res. **72,** 4643–4649 (1967).
5. C. Cox and W. Munk, "Statistics of the sea surface derived from sun glitter," J. Mar. Res. **13,** 198–227 (1954).
6. T. Takashima and Y. Takayama, "Emissivity and reflectance of the model sea surface for the use of AVHRR data of NOAA satellites," Pap. Meteorol. Geophys. **32,** 267–274 (1981).

7. K. Masuda, T. Takashima, and Y. Takayama, "Emissivity of pure and sea waters for the model sea surface in the infrared window regions," Remote Sensing Environ. **24,** 313–329 (1988).
8. C. François and C. Ottlé, "Estimation of the angular variation of the sea surface emissivity with the ATSR/ERS-1 data," Remote Sensing Environ. **48,** 302–308 (1994).
9. W. L. Smith, R. O. Knuteson, H. E. Revercomb, W. Feltz, H. B. Howell, W. P. Menzel, N. Nalli, O. B. Brown, J. Brown, P. J. Minnett, and W. McKeown, "Observations of the infrared radiative properties of the ocean—implications for the measurement of sea surface temperature via satellite remote sensing," Bull. Am. Meteorol. Soc. **77,** 41–51 (1996).
10. M. Born and E. Wolf, *Principles of Optics: Electromagnetic Theory of Propagation, Interference, and Diffraction of Light*, 6th ed. (Pergamon, New York, 1989), p. 38.
11. D. Clarke and J. F. Grainger, *Polarized Light and Optical Measurement* (Pergamon, New York, 1971), p. 55.
12. S. Khattak, R. A. Vaughan, and A. P. Cracknell, "Sunglint and its observation in AVHRR data," Remote Sensing Environ. **37,** 101–116 (1991).
13. G. M. Hale and M. R. Querry, "Optical constants of water in the 200-nm to 200-μm wavelength region," Appl. Opt. **12,** 555–563 (1973).
14. D. Friedman, "Infrared characteristics of ocean water (1.5–15 μ)," Appl. Opt. **8,** 2073–2078 (1969).
15. H. C. Blume, H. Huhnerfuss, and W. Alpers, "Variation of the microwave brightness temperature of sea surfaces covered with mineral and monomolecular oil films," IEEE Trans. Geosci. Remote Sensing **GE-21,** 295–300 (1983).
16. I. G. Ómuirgheartaigh and E. C. Monahan, "Statistical aspects of the relationship between oceanic whitecap coverage, wind speed, and other environmental factors," in *Oceanic Whitecaps and Their Role in Air-Sea Exchange Processes*, E. C. Monahan and G. M. Niocaill, eds. (Reidel, Dordrecht, 1986), pp. 125–128.
17. D. Lü, "Microwave radiation and remote sensing of natural surfaces," in *Principles of Microwave Radiation and Remote Sensing of the Atmosphere*, X. J. Zhou, ed. (Science, Beijing, 1982), p. 14.
18. F. J. Wentz, "A two-scale scattering model for foam-free sea microwave emission and backscattering from the sea surface," J. Geophys. Res. **80,** 3441–3446 (1975).
19. R. J. Wagner, "Shadowing of randomly rough surfaces," J. Acoust. Soc. Am. **41,** 138–148 (1967).
20. R. A. Brockelman and T. Hagfors, "Note on the effect of shadowing on the backscattering of waves from a random rough surface," IEEE Trans. Antennas Propag. **14,** 621–626 (1966).
21. K. E. Hamilton, "An experimental investigation of the shadowing of random rough surfaces," M.A. thesis (University of Colorado, Boulder, Colorado, 1966).
22. K. Yoshimori, K. Itoh, and Y. Ichioka, "Thermal radiative and reflective characteristics of a wind-roughened water surface," J. Opt. Soc. Am. A **11,** 1886–1893 (1994).
23. K. Yoshimori, K. Itoh, and Y. Ichioka, "Optical characteristics of a wind-roughened water surface: a two-dimensional theory," Appl. Opt. **34,** 6236–6247 (1995).
24. K. Masuda, Meteorological Research Institute, 1-1 Nagamine, Tsukuba, Ibaraki 305, Japan (personal communication).
25. H. Tan and S. Tian, *FORTRAN Language* (Qinghua, Beijing, 1981), p. 139.
26. J. Otterman, J. Susskind, G. Dalu, D. Kratz, and I. L. Goldber, "Effects of water-emission anisotropy on multispectral remote sensing at thermal wavelengths of ocean temperature and of cirrus clouds," Appl. Opt. **31,** 7633–7646 (1992).
27. P. Watts, M. Allen, and T. Nightingale, "Sea surface emission and reflection for the Along Track Scanning Radiometer," J. Atmos. Oceanic Technol. **13,** 126–141 (1996).
28. L. Pontier and C. Dechambenoy, "Détermination des constantes optiques de l'eau liquide entre 1 et 40 μ. Application au calcul de son pouvoir réflecteur et de son émissivté," Ann. Geophys. **22,** 633–641 (1966).
29. D. J. Segelstein, "The complex refractive index of water," M.S. thesis (University of Missouri, Kansas City, Missouri, 1981).
30. D. M. Wieliczka, S. Weng, and M. R. Querry, "Wedge shaped cell for highly absorbent liquids: infrared optical constants of water," Appl. Opt. **28,** 1714–1719 (1989).
31. R. G. Fleagle and J. A. Businger, *An Introduction to Atmospheric Physics*, 2nd ed. (Academic, New York, 1980), p. 210.